NANO LETTERS

2007
Vol. 7, No. 6
1804−1808

Diffusion-Based Electron Thermometry Using a Three-Junction Single-Electron Transistor

L. J. Swenson, D. K. Wood, and A. N. Cleland*

Department of Physics, University of California at Santa Barbara, Santa Barbara, California 93106

Received February 22, 2007; Revised Manuscript Received April 20, 2007

ABSTRACT

We describe a new mK-range nanoscale thermometer, based on a unique three-junction radio frequency single-electron transistor. The three-junction geometry allows separation of the thermal and electronic pathways, providing a potentially significant reduction of measurement-induced Joule heating. A radio frequency embedding tank circuit allows very fast readout. We demonstrate electronic and thermal operation, supported by numerical simulations. Applications to minimal back-action calorimetry and bolometry are discussed.

The diffusion of electrons through a normal metal tunnel junction occurs at zero voltage bias, with equal transfer rates in both directions, inversely proportional to the junction resistance. If the metals are at the same temperature, no net transfer of energy occurs, but if the temperatures differ, there is a net transfer of energy from the hotter to the colder metal. If one of the metals is replaced by a superconductor, and the junction is biased immediately below the superconducting gap, diffusion of hot electrons from the normal metal to the superconductor can cool the normal metal below ambient temperature, providing a form of electronic refrigeration.[1,2] Here we describe a variant application of this principle where we use the diffusion of electrons from a normal metal into the superconducting island of a single-electron transistor, changing the conductance of the transistor, and thereby providing a form of passive thermometry, with minimal power dissipated in the normal metal volume while monitoring its temperature.

A passive thermometer would serve as an important addition to nanoscale calorimeters and bolometers. There are in principle only weak constraints on the size and therefore heat capacity of such devices, so that scaling to submicrometer dimensions, with the concomitant reduction in heat capacity, can provide significant improvements in the detection of extremely small amounts of energy. This could eventually be extended to allow, for example, single-photon detection in the case of a nanoscale bolometer. However, one very serious limitation on such scaling is set by the power dissipated when measuring the temperature of the energy absorber, as this measurement process typically deposits significant amounts of energy, directly or indirectly, in the calorimeter or bolometer volume. Nanoscale devices are especially sensitive to this effect, setting a significant limitation on their ultimate performance.

Another important consideration when using nanoscale energy absorbers is related to the rate of energy relaxation. At very low temperatures, the electrons in a normal metal decouple from the phonons. The electron thermal time constant is then given by $\tau = C_V/G_T$, where C_V is the electron heat capacity and G_T is the effective electron−phonon thermal conductance, set by the electron−phonon coupling strength. Both C_V and G_T scale with metal volume, so τ is independent of volume and is a temperature-dependent characteristic of the metal. This time constant is typically on the nanosecond to microsecond time scale at temperatures below 1 K, so that monitoring the electron temperature involves a high-speed measurement. Sensitive high-speed thermometers capable of monitoring the electron temperature have been demonstrated,[3−7] allowing dynamic measurements of the electron energy relaxation, but a simultaneously high-speed *and* sufficiently low-power dissipation thermometer remains a significant challenge.

To this end, we have developed a novel Coulomb-blockade-based thermometer, with potentially minimal power dissipation in the energy-sensitive volume of a calorimeter. This device is similar to a conventional single-electron transistor (SET) but uses three nanoscale tunnel junctions to contact the SET center island rather than the standard two-junction configuration. The third junction provides a path for the in-diffusion of hot electrons from a normal metal absorber, making the SET conductance sensitive to the temperature of the absorber. The device is fabricated with a superconducting nanoscale center island contacted by three tunnel junctions with normal metal counter electrodes,

10.1021/nl0704329 CCC: $37.00
Published on Web 05/05/2007

forming superconductor-insulator-normal metal (SIN) contacts and a capacitive gate. Two of the junctions define the main electrical path, with transport through the junctions yielding the standard SET response, with the capacitive gate modulating the electrical conductance with single-electron periodicity. The third SIN junction serves as the thermal pathway. The degree to which the hot electrons diffusing through this junction affect the SET conductance can be manipulated by changing the island potential with the gate, resulting in a thermometer with a controllable sensitivity and therefore controllable dynamic range. The electrical impedance of the thermal pathway can be made quite large to ensure minimal electronic currents, thus minimizing Joule heating of the calorimeter by the thermometer.

In this letter, we report measurements on two similar versions of this device. In the first implementation, all three junctions have similar tunneling resistance, and the device was used to characterize the low-frequency electrical properties of the three-junction single-electron thermometer. The second version of the device was used to characterize the thermal response of the thermometer and demonstrate its radio frequency performance. This second version was fabricated with two of the junctions having equal tunneling resistance, with the third junction, attached to a normal metal calorimeter with a volume of about 7 μm^3, having twice this resistance. We used a radio frequency (rf) tank circuit to monitor the device response, using a configuration similar to the radio frequency SET (rf-SET).[4,8] This allowed a few tens of nanoseconds time resolution, sufficiently fast to resolve the thermal response of the calorimeter when the latter was heated using short electrical pulses. We present measurements with and without thermal power applied to the calorimeter. Numerical simulations support our interpretation of the device operation.

A dc schematic of the first version of the device is shown in Figure 1a. The device comprised an aluminum central island, contacted by three submicrometer SIN tunnel junctions with copper counter electrodes on a GaAs substrate. The junctions and center island were defined using electron beam lithography and angled evaporation of aluminum, followed by oxidation and the copper counter electrode evaporation. External connections were made using Au wire bonds and the devices mounted on a dilution refrigerator operating at 25 mK.

Figure 1b shows current−voltage characteristics taken with this implementation, where each junction had a resistance $R_t \sim 100$ kΩ. The current I_1 through one junction was measured as its voltage V_1 was swept while holding the second junction's voltage V_2 and the gate electrode voltage V_g fixed; the third junction was grounded. V_2 was then stepped and the measurement repeated. When V_1 and V_2 are sufficiently small, I_1 is suppressed due to the combination of the superconducting gap $2\Delta \sim 360$ μeV and the Coulomb blockade, with $e^2/2C_\Sigma \sim 13$ μeV. By varying the gate voltage, the electrochemical potential of the island can be adjusted, allowing control of the Coulomb blockade. Figure 1d shows the differential conductance $G = \mathrm{d}I_1/\mathrm{d}V_1$ through the first junction as V_g is swept, with V_1 biased at the energy gap

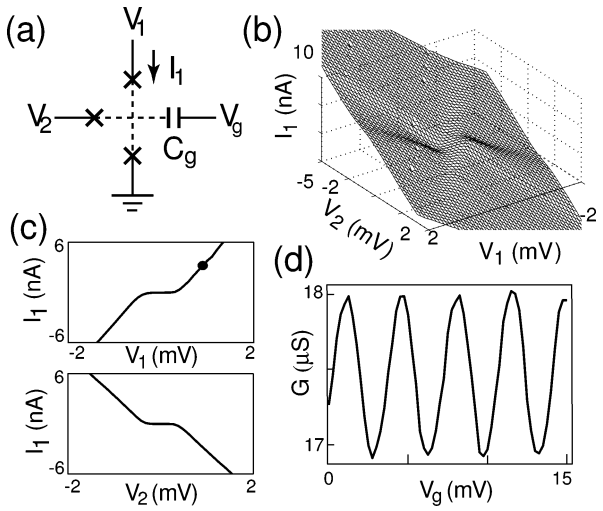

Figure 1. (a) Circuit schematic. Dashed traces are superconducting aluminum and solid traces are normal-metal copper. C_g is the gate capacitor, and the SET island comprises the crossed superconducting leads between the three junctions and C_g. (b) Stability plot. Current I_1 measured as a function of the voltages V_1 and V_2 with the gate voltage V_g held constant. (c) I_1 measured as a function of either V_1 (top) or V_2 (bottom) with the other voltage source grounded. V_g was also held at ground. The bullet (●) marks the operating point for measuring the differential conductance. (d) Differential conductance $G = \mathrm{d}I_1/\mathrm{d}V_1$ measured as a function of V_g.

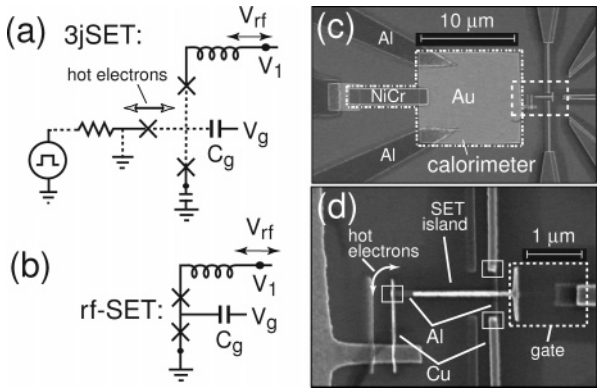

Figure 2. (a) Schematic for radio frequency measurements for the three-junction SET (3jSET) and (b) for a conventional rf-SET. Dashed traces are superconducting aluminum and solid traces are normal metal. (c) Device image showing Au−NiCr calorimeter (dash−dot box) and the three-junction SET (inside dashed border). (d) SET island in detail, with annotations for the gate capacitor, island, and small solid boxes around each of the three tunnel junctions. The location of the third junction, through which hot electrons diffuse, is also indicated.

and V_2 grounded. As with a conventional SET, the conductance is periodic in the gate voltage, with a period of one electron. Heating in the normal metal leads due to the current I_1 is minimal in these measurements.

To investigate the thermometric properties, we used the second device implementation, with $e^2/2C_\Sigma \approx 25$ μeV and $2\Delta \approx 360$ μeV, with tunnel resistances in the range of 100−200 kΩ. A measurement schematic and image of the device are shown in Figure 2. One junction, with tunnel resistance $R_t \approx 100$ kΩ, was grounded at rf (>1 MHz), but the quasi-dc voltage was controllable. The second junction ($R_t \approx 100$ kΩ) was connected to a rf tank circuit that included a $L =$

470 nH inductor, which with the stray capacitance $C \approx 0.65$ pF had a resonance frequency of $f = 1/2\pi\sqrt{LC} = 287$ MHz. The tank circuit provides an approximate impedance match to the 50 Ω cabling, allowing large bandwidth reflectometry similar to the rf SET.[4,8] The third junction served as the thermal diffusion channel, had resistance $R_t \approx$ 190 kΩ, and was connected to a submicrometer gold island (volume $10 \times 10 \times 0.05$ μm^3), which was in turn attached to a 50 Ω NiCr resistor (volume $8 \times 1.7 \times 0.1$ μm^3); the combined gold and NiCr volumes comprise our nanoscale calorimeter. The gold pad was electrically grounded using two aluminum electrodes. The superconducting aluminum is a poor thermal conductor so that it does not provide a thermal path for cooling. The other end of the NiCr resistor was connected via thermally insulating aluminum electrodes to a gold wire bond pad, to which we could apply short electrical heat pulses.

A fixed-frequency rf signal, applied through a directional coupler to the tank circuit, is reflected from the device by an amount that depends sensitively on the source frequency and on the differential electrical conductance G of the device to ground. Operated at the resonant frequency of the tank circuit, the reflection coefficient ρ is approximately given by

$$\rho = \frac{GL/C - Z_0}{GL/C + Z_0} \tag{1}$$

where $Z_0 = 50$ Ω. Monitoring the reflectance ρ allows us to measure the SET conductance G, here with a measurement bandwidth of 17 MHz. The calorimetric NiCr resistor is heated by applying short voltage pulses, heating the electrons in the calorimeter, with the pulse kept short to ensure that only local (electron) heating occurs. The time for the heat pulse in the NiCr to be distributed to the gold part of the calorimeter is estimated to be less than 200 ps. Some hot electrons in the calorimeter will have sufficient thermal energy to overcome the Coulomb blockade and superconducting gap in the island and can thus tunnel into the SET island. This changes the differential conductance of the SET, detected as a change in its rf reflectance. With the superconducting wires inhibiting thermal transport, the dominant path for cooling of the hot calorimeter electrons is through electron−phonon relaxation;[9−12] monitoring the time dependence of the relaxation of the SET conductance allows us to measure the electron−phonon time constant.

We mapped out the thermal response of the device as a function of bias V_1 and gate voltage V_g, using a fixed 5 μs long, 15 nW (75 fJ) heat pulse. The result of this measurement is shown in Figure 3a, plotting the change in the reflection coefficient $\Delta\rho$ as a function of V_1 and V_g. A numerical simulation of the thermometer response, modeled under the same conditions, is shown in Figure 3b. The simulation used a modified version of the open-source program MOSES, a Monte Carlo-based simulator for single-electron circuits.[13−15] MOSES is applicable to normal-metal devices, where the calculation of the junction tunneling probabilities at uniform temperature has an analytic solution.

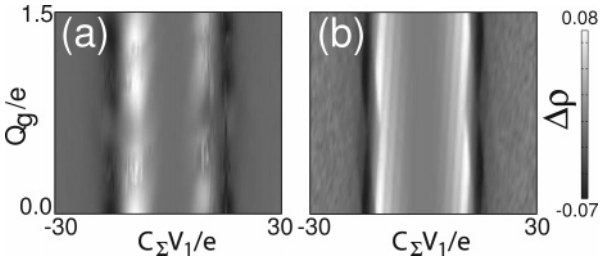

Figure 3. (a) Measured change $\Delta\rho$ in reflectance due to temperature change $\Delta T \sim 4\ e^2/2k_B C_\Sigma$ induced by a 75 fJ heat pulse as a function of bias $C_\Sigma V_1$ and gate charge $C_g V_g$. (b) Simulated change $\Delta\rho$ due to equivalent temperature rise as in (a), with same axes.

We modified MOSES in order to allow for unequal temperatures and SIN tunneling, requiring numerical integration to extract the tunneling probabilities.[16]

An important parameter for the simulation is the calorimeter electron temperature achieved during the heat pulse. We assume electron−phonon coupling is the thermal bottleneck, as is typically the case in small metal islands below 1 K, in which case the thermal power from the electrons to the phonons P is approximately given by[9−11]

$$P \approx \Sigma V(T^5 - T_0^5) \tag{2}$$

where V is the volume of normal metal in the calorimeter (6.9 μm^3), $\Sigma \sim 10^9$ W/m^3-K^5 is the electron−phonon coupling constant, T the electron temperature, and T_0 the phonon temperature. A 15 nW pulse gives a steady-state electron temperature $T \sim 1.1$ K $\sim 4e^2/2C_\Sigma$. One feature common to both the experimental and simulated results is that, as expected, the thermometric response is periodic with gate voltage, with a period of one electron.

By measuring the differential conductance of the device and its response to a fixed heat pulse, the optimal operating point, in terms of V_1 and V_g, can be determined. The measured differential conductance G as a function of V_1 is shown in Figure 4a. The measurement was performed at 25 mK with no heating on the calorimeter, with conductance normalized to the conductance G_m that achieves impedance matching in the reflectometer. The corresponding reflectometer response is shown in Figure 4b. The greatest response occurs in the region of Coulomb blockade at the edge of the superconducting gap, where there is a large thermally induced change in the differential conductance G. Numerical simulations are shown in Figure 4c,d. With V_1 just below the combined Coulomb blockade and superconducting gap, an increase in the calorimeter temperature yields an increased G and a decrease in reflected signal amplitude. However, for V_1 above this voltage, G decreases upon heating, yielding an increased reflection. A plot of the simulated differential conductance below the gap, as a function of V_g, is shown in Figure 4e, with no heating of the calorimeter. By comparing this with the heating response, shown in Figure 4f, it is clear that the optimal gate bias is at a value of minimal conductance, allowing for the greatest increase in conductance upon heating the calorimeter.

Having established the optimal V_1 and V_g, we investigated the response as a function of calorimeter temperature, which

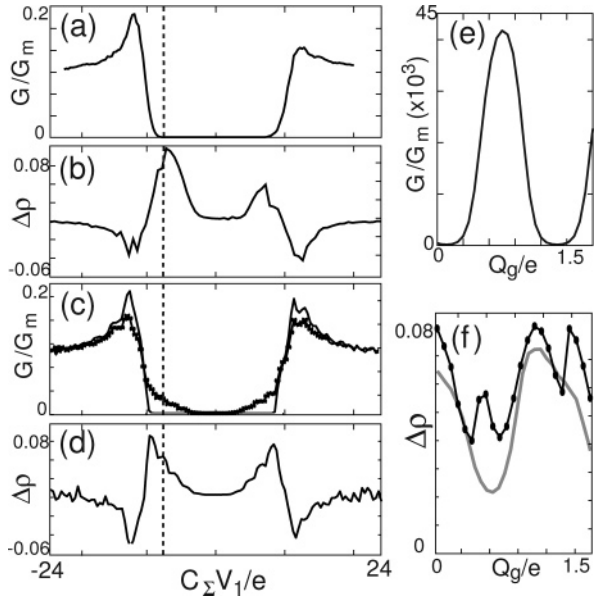

Figure 4. (a) Measured differential conductance at 25 mK. (b) Measured change in reflectance ρ due to a fixed 15 nW, 5 μs heat pulse, vs bias V_1. (c) Simulated differential conductance with calorimeter at base temperature (solid) and heated by 4 $e^2/2C_\Sigma$ (crosses). (d) Simulated change in ρ due to heating to 4 $e^2/2C_\Sigma$; (a−d) are for a gate voltage giving maximum response. (e) Simulated differential conductance as function of gate charge C_gV_g. (f) Measured (●) and simulated (gray) change in ρ due to heating calorimeter by $4e^2/2C_\Sigma$. In (e) and (f), V_1 is biased just below gap, indicated by the dashed line in (a−d).

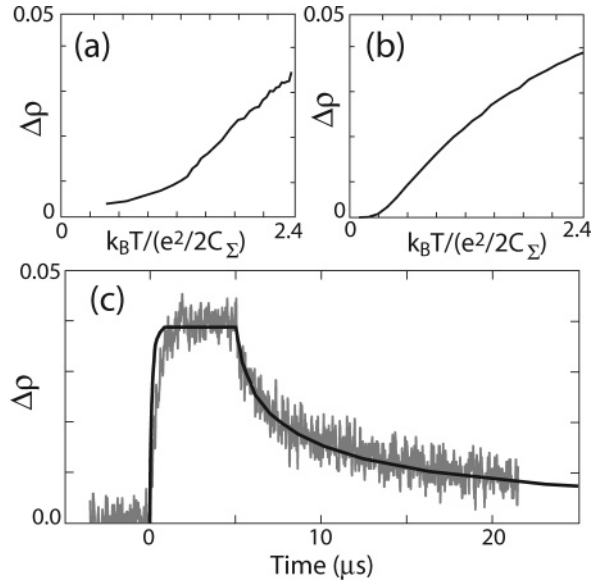

Figure 5. (a) Measured change in ρ as a function of calorimeter temperature, controlled by adjusting the amplitude of the voltage pulse applied to the heater. (b) Simulated change in ρ. (c) Measured time domain response to a 5 fJ heat pulse. Solid curve is fit as discussed in the text.

was adjusted by varying the pulse amplitude applied to the heater. In Figure 5a, the measured response is displayed. Figure 5b shows the simulated response for the same calorimeter temperature range. We then use the time resolution of the rf-coupled SET to monitor the calorimeter response after a heat pulse. This is shown for a 5 μs long, 1 nW (5 fJ) heat pulse in Figure 5c. We can calculate the expected time dependence by convolving the simulated temperature dependence $\Delta\rho(T)$, with the temperature as a function of time $T(t)$. When the pulse is turned on, the latter function is predicted by combining eq 2 with the Sommerfeld heat capacity, $C_e = \gamma VT$, where γ is a composite Sommerfeld constant for this calorimeter,[4] yielding

$$\frac{dT}{dt} = \frac{\Sigma}{\gamma T}\left(\frac{P_{in}}{\Sigma V} - T^5 + T_0^5\right) \quad (3)$$

For the decay pulse, the input power P_{in} is zero and this equation reduces to:

$$\frac{dT}{dt} = -\frac{\Sigma}{\gamma T}(T^5 - T_0^5) \quad (4)$$

Integrating these expressions with the known heat pulse produces the solid line in Figure 5c, with fit electron−phonon coupling constant $\Sigma \approx 1.1 \times 10^9$ W/m^3-K^5, in reasonable agreement with other measurements.[4]

An important aspect of the three-junction geometry is that in principle no net measurement current flows through the calorimeter itself. If an electrically grounded calorimeter is used, some current will flow through it due to the bias or rf power applied to the SET. However, if the tunnel resistance of the junction calorimeter is significantly larger than that of the other junctions, most of this current flow will pass through the other junctions, decreasing the heat deposited in the calorimeter. Alternatively, in a bolometric configuration, the calorimeter can be decoupled from ground and heat coupled by collecting electromagnetic infrared radiation using a superconducting antenna. In this configuration, essentially no net measurement current will flow through the calorimeter junction, so no measurement power is dissipated in the calorimeter, significantly decreasing the minimum temperatures achievable.

It is useful to estimate the smallest detectable signal for this device, which is admittedly not optimized. Taking into consideration the 6 K noise temperature of our cryogenic preamplifier, and a typical rf signal of −100 dBm at the tank circuit, the calculated minimum detectable change in temperature of the calorimeter is ∼200 μK/Hz$^{1/2}$, dominated by the preamplifier noise. We can compare this with other approaches to measuring normal metal electron temperature. One method is provided by the superconductor-insulator-normal metal (SIN) tunnel junction, with a temperature sensitivity of ∼280 μK/Hz$^{1/2}$,[5] comparable to the 3jSET. The measurement bandwidths are also comparable, as both can be rf-coupled to achieve bandwidths of ∼10^8 Hz. However, the SIN thermometer dissipates power directly in the normal metal it is measuring, Joule heating the electrons; at temperatures below 1 K, this is a significant disadvantage, typically preventing the electrons from cooling below about 100 mK. In the 3jSET, this power can in principle be reduced to zero, allowing the electrons to cool to the ambient temperature (this was not achieved here, as our electronic

configuration did not block either rf or dc power through the calorimeter-sensing tunnel junction). Another related instrument is the proximity-coupled superconductor-normal metal-superconductor junction,[17] for which noise figures have not been reported, but which also dissipates dc power to perform the measurement. An in-principle nondissipative approach is to use noise thermometry, with the best signal-to-noise achieved using a dc SQUID.[10,12] Noise-based temperature measurements are not directly comparable to the 3jSET in terms of sensitivity. However, the measurement bandwidth is significantly smaller than in the 3jSET- or SIN-based measurements, so this approach is not applicable to the pulsed temperature changes we are measuring here. We note that the temperature resolution achieved here can be significantly improved by designing a better impedance match, leading to greater sensitivity to conductance changes and thus temperature changes in the calorimeter. Finally, because the coupling of the rf measurement power to the calorimeter can be significantly reduced by device design, the rf measurement power could be significantly increased without causing heating of the calorimeter, leading to even greater temperature sensitivity; we estimate sensitivities of order $1-10\ \mu\mathrm{K/Hz^{1/2}}$ should be achievable.

In conclusion, we have investigated a novel thermometer based on a three-junction SET, where temperature changes in a calorimeter modulate the SET conductance due to the diffusion of hot electrons from the calorimeter. We have demonstrated thermometry with nanosecond scale time resolution and a temperature sensitivity of $\sim 200\ \mu\mathrm{K/Hz^{1/2}}$. Future efforts are directed at reducing the calorimeter volume, increasing the electrical impedance of the thermal pathway to reduce Joule heating due to leakage current from the electrical pathway and attempting to couple energy via a THz-frequency antenna.

Acknowledgment. This work was supported in part by the NASA Office of Space Science under grant NAG5-11426 and by the DMEA Center for Nanoscience Innovation for Defense.

References

(1) Manninen, A. J.; Suoknuuti, J. K.; Leivo, M. M.; Pekola, J. P. *Appl. Phys. Lett.* **1999**, *74*, 3020−3022.
(2) Giazotto, F.; Heikkila, T. T.; Luukanen, A.; Savin, A. M.; Pekola, J. P. *Rev. Mod. Phys.* **2006**, *78*, 217.
(3) Kauppinen, J. P.; Loberg, K. T.; Manninen, A. J.; Pekola, J. P.; Voutilainen, R. A. *Rev. Sci. Instrum.* **1998**, *69*, 4166.
(4) Schmidt, D. R.; Yung, C. S.; Cleland, A. N. *Phys. Rev. B* **2004**, *69*, 140301(R).
(5) Schmidt, D. R.; Yung, C. S.; Cleland, A. N. *Appl. Phys. Lett.* **2003**, *83*, 1002.
(6) Yung, C. S.; Schmidt, D. R.; Cleland, A. N. *Appl. Phys. Lett.* **2002**, *81*, 31.
(7) Knuuttila, T. A.; Nummila, K. K.; Yao, W.; Kauppinen, J. P.; Pekola, J. P. *Physica E* **1998**, *3*, 224.
(8) Schoelkopf, R. J.; Wahlgren, P.; Kozhevnikov, A. A.; Delsing, P.; Prober, D. E. *Science* **1998**, *280*, 1238.
(9) Little, W. A. *Can. J. Phys.* **1959**, *37*, 334.
(10) Wellstood, F. C.; Urbina, C.; Clarke, J. *Phys. Rev. B* **1994**, *49*, 5942.
(11) Gantmakher, V. F. *Rep. Prog. Phys.* **1974**, *37*, 317.
(12) Schwab, K.; Henriksen, E. A.; Worlock, J. M.; Roukes, M. L. *Nature* **2000**, *404*, 974.
(13) Chen, R. H. *Meeting Abstracts, Fall Meeting, San Antonio, TX*; The Electrochemical Society; Pennington, NJ, 1996; Vol. 96-2, p 576.
(14) Averin, D. V.; Likharev, K. K. *J. Low Temp. Phys.* **1986**, *62*, 345.
(15) Chen, R. H.; Korotkov, A. N.; Likharev, K. K. *Appl. Phys. Lett.* **1996**, *68*, 1954.
(16) Wasshuber, C. *Computational Single-Electronics*; Springer-Verlag: New York, 2001.
(17) Jiang, Z.; Lim, H.; Chandrasekhar, V.; Eom, J. *Appl. Phys. Lett*. **2003**, *83*, 2190−2192.

NL0704329